Resonant inelastic light scattering in crystals

M. M. Sushchinskiĭ

P. N. Lebedev Physics Institute, Academy of Sciences of the USSR
Usp. Fiz. Nauk **154**, 353–379 (March 1988)

The author develops theoretical methods applicable to light scattering in dispersive absorbing crystals. Special attention is paid to scattering with widely different absorption at incident and scattered frequencies that generates frequency shifted radiation (hyperresonance). Different types of scattering are considered: Raman scattering, hyper-Raman and hyper-Rayleigh scattering, and stimulated Raman scattering. Experimental data on scattering in crystalline powders, films, single crystals, and near-surface crystal layers are analyzed.

TABLE OF CONTENTS

1. INTRODUCTION

The general problem of nonlinear optical phenomena in dispersive media is of undoubted interest. A number of studies treated nonlinear processes in connection with the creation of optical quantum generators in a dispersive active medium, with scattering from medium inhomogeneities serving as a nonresonant feedback mechanism. Several experimental and theoretical investigations addressed stimulated Raman scattering (SRS) in crystalline powders and turbid liquids.[1-11]

This review is devoted to the study of nonlinear processes—hyper-Rayleigh (HRLS) and hyper-Raman (HRS) scattering, as well as spontaneous Raman scattering (RS) and SRS—in crystals, which in practice are always macroscopically inhomogeneous and absorptive. This is particularly true of the near-surface layers in crystals after some form of technological processing. In the course of processing, various types of inhomogeneities are created in the near-surface layers. These inhomogeneities can markedly influence the processes occurring in such layers. The study of various types of light scattering in near-surface semiconductor layers is of special interest since these layers are used in microelectronics.

In recent times, picosecond and femtosecond probe pulses have been successfully employed to study processes in near-surface layers that evolve quite rapidly under the influence of strong laser radiation (see Ref. 12). These research methods are based on the analysis of intensity and polarization of the second optical harmonic generation (SHG) in the surface layer of the crystal. Because of the greater or lesser dispersion in the near-surface layer it is useful to consider HRLS in addition to SHG. These two processes are essentially different, although both produce radiation at the frequency $\omega' = 2\omega$, where ω is the frequency of the incident radiation. Second harmonic generation is a coherent process and therefore the amplitudes of the generated secondary radiation at frequency 2ω are added to the wave of frequency ω passing through a thin, plane-parallel layer of a nonlinear crystal. These amplitudes are proportional to the thickness l of the layer (at small l) and the intensity of SHG is proportional to l^2. In contrast, in a dispersive medium the coherence of 2ω radiation is destroyed by the random phase jumps of waves whose direction changes repeatedly. Accordingly, the intensities of the waves add and the total intensity of scattered radiation at the same frequency 2ω is proportional to the thickness l of the scattering layer (rather than l^2).[1)]

Hyper-Raman processes, SRS, as well as spontaneous RS, exhibit this same dependence on the thickness of the scattering layer. Consequently these problems can be considered within the same framework, using a common mathematical apparatus.

Light scattering is often studied near the intrinsic absorption band of a crystal. Then the absorption coefficients for the incident and the frequency-shifted radiation are unequal. In the case of spontaneous RS and SRS this difference is generally small and can usually be neglected. But even a small difference in the absorption coefficients at frequencies ω and ω' is significant in some light scattering processes. For this reason in both the experimental and theoretical sections of this article we systematically take into account the different properties of the medium at incident and scattered frequencies when analyzing inelastic light scattering.

Different absorption of radiation at ω and ω' is typical in HRLS and HRS, where the frequency shift of scattered radiation is large. When studying these processes researchers often fall into the opposite extreme and unjustifiably ig-

 0038-5670/88/030181-15$01.80

nore absorption of the incident radiation ω. The general approach developed in this article allows us to analyze the true role of incident frequency absorption in HRLS and HRS processes.

A sizeable difference in light absorption at incident and scattered frequencies is often also observed in the spontaneous RS and SRS near the intrinsic absorption band of the crystal. We shall lump these different light scattering mechanisms into a single category of "hyperresonant" light scattering. Whether a given type of scattering should be considered "hyperresonant" depends on the particular experimental parameters.

2. OPPOSING FLUXES

In order to solve the general problem of light scattering in dispersive media we must derive and analyze the transport equations. Because of the great complexity of these equations we employ approximate methods of analyzing light propagation in dispersive media that are based on crude but graphic models of the associated phenomena.

First, let us simplify the geometry of the problem. We treat the scattering medium as an infinite plane-parallel layer of thickness l. Then we assume that the entire surface of this layer is uniformly irradiated by a diffuse light source. In practice a laser beam is usually employed and only a limited region of the scattering layer's surface is irradiated by a parallel or weakly focused beam. It is the case, however, that in strongly dispersive media a flat surface element of thickness dx located at a not-too-large depth x can be considered as irradiated by diffuse light, regardless of the illumination method.

We define a plane parallel to the layer boundaries at a distance x from the irradiated surface (Fig. 1). Because of scattering this plane will be illuminated both from above and below. Let $n_1(x)$ and $n_2(x)$ be the numbers of excitation photons of frequency ω that propagate up and down respectively, and let $n_1'(x)$ and $n_2'(x)$ be the numbers of photons of shifted frequency ω' that propagate in those same directions. Light is absorbed and scattered in the layer dx, and frequency-shifted ω' light is generated there. Consequently the photon numbers n_1, n_2, n_1', n_2' change.

The medium is question can be described by a constant s, which characterizes the flux reflected by an infinitely thin layer, an absorption coefficient[2] k and a nonlinear susceptibility χ (or scattering cross-section $\varkappa$). If we consider the photon balance in our dispersive layer under the assumption that the light intensity of frequency ω' is much smaller than the intensity of the original ω radiation, we arrive at the following system of equations for $n_1(x)$ and $n_2(x)$:

$$\frac{dn_1}{dx} = -(s+k)\,n_1 + sn_2, \tag{1}$$

$$\frac{dn_2}{dx} = -sn_1 + (s+k)\,n_2. \tag{2}$$

The above system of equations has a general solution of the form

$$n_1 = \bar{C}_1 e^{Lx} + \bar{C}_2 e^{-Lx}, \tag{3}$$

$$n_2 = R^{-1}\bar{C}_1 e^{Lx} + R\bar{C}_2 e^{-Lx}; \tag{4}$$

where $L = (k^2 + 2ks)^{1/2}$, $R = (s + k - L)/s$. We assume that $n_1(x) \ll n_0$, $n_2(x) \ll n_0$, where n_0 is the initial photon flux of frequency ω incident upon the layer.

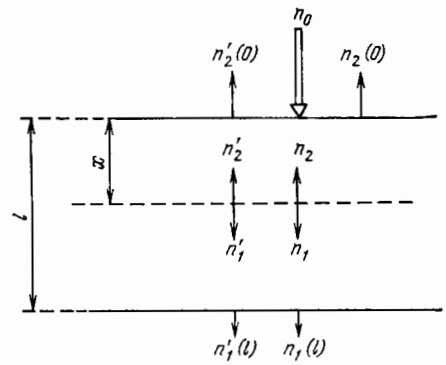

FIG. 1. Photon flux diagram in a flat layer of crystalline powder.

Given the boundary conditions

$$n_1(0) = n_0, \quad n_2(l) = 0 \tag{5}$$

we have

$$\bar{C}_1 = -R^2 n_0 e^{-2Ll} M^{-1}, \quad \bar{C}_2 = n_0 M^{-1}, \quad M = 1 - R^2 e^{-2Ll}. \tag{6}$$

The measured photon flux in the "transmission" scheme is $n_1(l)$; in the "reflection" scheme it is $n_2(0)$. For these quantities we obtain

$$n_1(l) = \bar{C}_2 (1 - R^2)\, e^{-Ll}, \tag{7}$$

$$n_2(0) = R\bar{C}_2 (1 - e^{-2Ll}). \tag{8}$$

It follows from (7) and (8) that R represents the reflection coefficient appropriate to an infinitely thick layer of the medium and L is the effective damping coefficient. The effective parameters L and R can be easily extracted from experimentally measured values of $n_1(l)$ and $n_2(0)$ for several layer thicknesses l; the constants s and k can be evaluated accordingly. We note that these parameters can change strongly depending on the experimental conditions, particularly if the sample is heated or a phase transition is approached. In such experiments the properties of the medium should be systematically controlled.

In the one-dimensional opposing fluxes model equations similar to (1) and (2) can be derived for the secondary radiation of frequency ω'. This model has been successfully applied to SRS in Refs. 2–4. If we take into account the changes in the numbers of photons occurring in a layer of thickness dx as a result of HRLS,HRS, SRS, and RS processes, we find

$$\frac{dn_1'}{dx} = -(s' + k')\,n_1' + s'n_2' + \varphi_1(x), \tag{9}$$

$$\frac{dn_2'}{dx} = -s'n_1' + (s' + k')\,n_2' + \varphi_2(x); \tag{10}$$

where s' and k' are constants [analogous to the s and k of equations (1)–(8)] that describe the scattering and absorption effectiveness of the medium at frequency ω'. Equations (9) and (10) should be solved with the boundary conditions

$$n_1'(0) = 0, \quad n_2'(l) = 0, \tag{11}$$

where l is the layer thickness. The actual form of the functions $\varphi_1(x)$ and $\varphi_2(x)$ depends on the scattering process.

Note that in all cases the medium can be described by the effective parameters

$$L' = (k'^2 + 2k's')^{1/2}, \quad R' = (s' + k' - L')(s')^{-1}. \quad (12)$$

In HRS and HRLS processes a large difference between ω and ω' (with $\omega' > \omega$) typically ensures that $L' \gg L$. In RS and SRS processes in the Stokes regime (at large vibrational frequencies) the opposite inequality, $L' \ll L$, is quite possible. If either of these inequalities applies we shall consider the process hyperresonant.

The system of equations (9) and (10) is a system of nonhomogeneous, linear differential equations with constant coefficients.

We shall present the solutions of this system for RS and related scattering processes.

2.1. Raman scattering

In this case

$$\varphi_1 = B(n_1 + n_2), \quad \varphi_2 = -B(n_1 + n_2) = -\varphi_1, \quad (13)$$

where B is a quantity proportional to the RS cross-section. After simple but tedious calculations we obtain the following expressions for the quantities $n_1'(l)$ and $n_2'(0)$, that determine the measured RS intensities in the "transmission" and "reflection" schemes respectively:

$$n_1'(l) = \frac{Bn_0(1+R)(1+R')}{MM'}\left\{\frac{e^{-L'l} - e^{-Ll}}{L - L'}[1 - RR'e^{-(L+L')l}] - \frac{1 - e^{-(L+L')l}}{L + L'}(Re^{-Ll} + R'e^{-L'l})\right\}, \quad (14)$$

$$n_2'(0) = \frac{Bn_0(1+R)(1+R')}{MM'}\left\{\frac{1 - e^{-(L+L')l}}{L + L'}[1 + RR'e^{-(L+L')l}] - \frac{e^{-L'l} - e^{-Ll}}{L - L'}(Re^{-Ll} - R'e^{-L'l})\right\}, \quad (15)$$

If the thickness l of the scattering layer is small ($Ll \ll 1$; $L'l \ll 1$)

$$n_1'(l) = n_2'(0) = \frac{Bn_0(1 + RR' - R - R')}{(1-R)(1-R')}l. \quad (16)$$

i.e., the RS intensity in both the "transmission" and "reflection" schemes is proportional to the scattering layer thickness and is only weakly dependent (via the coefficients R and R') on the absorption and scattering properties of the medium. Therefore, when the resonance excitation conditions are approached, the coefficient B, and consequently the RS intensity, increase sharply. As l increases, absorption and macroscopic scattering in the medium become more and more important, but the RS intensity continues to increase until the thickness reaches l_M, which corresponds approximately to the maximum of the function

$$\Psi(l) = \frac{e^{-L'l} - e^{-Ll}}{L - L'} - \frac{R'e^{-L'l} - Re^{-Ll}}{L - L'}. \quad (17)$$

Given optimal conditions for the measurement of RS intensity in the "transmission" scheme, this quantity equals

$$n_1'(l_M) = \frac{n_0(1+R)(1-R')(1-R')}{MM'}\frac{B}{L}. \quad (18)$$

We shall discuss this relation further in the following section.

When the scattering layer is thick ($l \to \infty$, bulk samples), $n_2'(0)$ tends towards its maximum value, proportional to $B/L + L'$), whereas $n_1'(l)$ falls off exponentially. The quantity $n_1'(x)$ has a maximum of depth x_M determined by the condition [see (17)]

$$x_M = \frac{\ln(L/L')}{L - L'}. \quad (19)$$

Up to this point we have assumed that $L' \neq L$. The $L' = L$ case requires separate treatment. Here we find

$$n_{10}'(l) = \frac{Bn_0(1+R)^2 e^{-Ll}}{M^2}\left[l(1 + R^2e^{-2Ll}) - \frac{R}{L}(1 - e^{-2Ll})\right]. \quad (20)$$

$$n_{20}'(0) = \frac{Bn_0(1+R)^2}{M^2}\left[\frac{1 - e^{-2Ll}}{2L}(1 + R^2e^{-2Ll}) - 2RLe^{-2Ll}\right]. \quad (21)$$

If the layer is thin ($Ll \ll 1$) we have

$$n_{10}'(l) = n_{20}'(0) = Bn_0 l.$$

In the general case, the condition for $n_{10}'(l)$ to reach its maximum is

$$l_{M0} = \frac{1+R}{L} \approx \frac{1}{L}. \quad (22)$$

Thus, approximately

$$n_{10}'(l_{M0}) = \frac{Bn_0(1+R)^2(1-R)}{eLM^2}. \quad (23)$$

Comparing (23) with (18) we find that in the $L' \approx L$ case the RS intensity in the "transmission" scheme is smaller by a factor of e than in the hyperresonance case, given optimal layer thickness.

In bulk samples, i.e., at large l ($Ll \gg 1$), we can carry out calculations analogus to those for the $L' \neq L$ case and obtain

$$n_{10}'(x) = b_0 x e^{-Lx}. \quad (24)$$

This quantity has a maximum at

$$x_{M0} = L^{-1}. \quad (25)$$

Comparing this result with (19) we observe that the effective layer depth for the hyperresonant RS process is larger by a factor of $\ln(L/L')$ than the corresponding quantity for the ordinary RS conditions (i.e., where $L' \approx L$).

2.2. Hyper-Raman and hyper-Rayleigh light scattering

Since the intensities of HRS and HRLS processes are analogously dependent on the intensity of the exciting radiation and both processes are noncoherent, the following results apply to both of these types of scattering. For simplicity we shall discuss HRS in this section. We note that the term "hyper-Rayleigh scattering" is imprecise because macroscopic inhomogeneities of the medium contribute to the scattering. However, if the extent of the inhomogeneity is small, this process is indeed similar to Rayleigh scattering, although the generation of secondary radiation within each microcrystal follows the SHG mechanism.

The expression for the HRS intensity is structurally identical to the well-known RS intensity formula

$$I_{HRS} = C\left|\sum_{\rho\sigma} e_\rho^s \beta_{\rho\sigma\sigma} e_\sigma^i e_\sigma^i\right|^2 I_0^2, \quad (26)$$

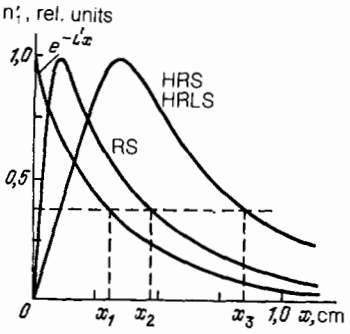

FIG. 2. Radiation intensity dependence in RS, HRS, and HRLS on the layer thickness of a dispersive medium (x_1, x_2, x_3 are the effective depths for light scattering processes indicated in the figure).

where C is a proportionality coefficient; e^i_σ, e^s_σ are the unit polarization vector components of the incident and scattered electric fields; $\beta_{\rho\sigma\sigma}$ are the HRS tensor components; I_0 is the intensity of the incident radiation. There exists an analogous expression for HRLS. A more detailed analysis of this expression will be carried out in the next section in connection with hyperresonace conditions. At this point it is important that the HRS and HRLS intensities are quadratically dependent on the photon density of the incident radiation:

$$I_{\text{HRLS}} = an_0^2, \quad I_{\text{HRS}} = a'n_0^2.$$

Consequently, for HRS in the opposing fluxes model, the functions $\varphi_1(x)$ and $\varphi_2(x)$ that appear in (9) and (10) have the form

$$\varphi_1(x) = \beta(n_1^2 + \gamma n_2^2), \qquad (27)$$
$$\varphi_2(x) = -\beta(\gamma n_1^2 + n_2^2);$$

where γ is a quantity that characterizes the HRS indicatrix; the coefficients s' and k' describe the scattering and absorption properties of the medium at frequency 2ω (HRLS) or $2\omega \pm \omega_k$ (HRS); ω_k is the vibrational frequency of the crystal).

Calculation of HRLS and HRS intensities are analogous to those carried out earlier for the RS case with $L' \neq L$. Omitting ponderous intermediate steps we only cite the approximate formulas, where we define

$$a = \frac{\beta n_0^2 R'}{M'M^2}, \quad b = \frac{1+\gamma R^2}{R'} + \gamma + R.$$

Then we have

$$n'_{1\text{H}}(l) = \frac{ab}{L'-2L}(e^{-2Ll} - e^{-L'l}). \qquad (28)$$

For the optimal thickness l_{MH} in the "transmission" scheme we obtain

$$l_{\text{MH}} = \frac{\ln(L'/2L)}{L'-2L}, \qquad (29)$$

which yields

$$n'_{1\text{H}}(l_{\text{MH}}) = \frac{ab}{L'}\exp\left(-\frac{2L}{L'-2L}\ln\frac{L'}{2L}\right) \approx \frac{ab}{L'}. \qquad (30)$$

The peak value $n'_{1\text{H}}$ inside the sample is achieved at

$$x_{\text{MH}} = \frac{\ln(L'/2L)}{L'-2L}. \qquad (31)$$

According to (31) the effective hyperscattering depth l_{eff} is much greater than the effective depth of linear processes of absorption and RS at $L' \approx L$, in which case $l_{\text{eff}} \sim 1/L$. In Fig. 2 we plot the intensity of radiation scattered by indicated processes against the layer depth in a dispersive absorbing medium.

HRLS and HRS obey numerous "selection rules." For example, HRLS is forbidden in centrosymmetric crystals. Still, HRLS is observed in such crystals as well. This deviation from the HRLS selection rule is probably due to lattice deformations which produce noncentrosymmetric regions in centrosymmetric crystals.

The authors of Ref. 15 proposed quadrupole polarization as a HRLS source in centrosymmetric crystals. We believe quadrupole polarization can make but a small contribution to HRLS in a medium with significant optical inhomogeneities.

2.3. Stimulated Raman scattering

In the SRS case the equations of the opposing fluxes model have the form (see Refs. 2, 3):

$$\frac{dn'_1}{dx} = -(s'+k')n'_1 + s'n'_2 + B(n_1+n_2) + An'_1(n_1+\gamma_1 n_2), \qquad (32)$$

$$\frac{dn'_2}{dx} = -s'n'_1 + (s'+k')n'_2 - B(n_1+n_2) - An'_2(\gamma_1 n_1 + n_2); \qquad (33)$$

where A and γ_1 are coefficients that characterize the SRS process and the rest of the notation is from the preceeding sections. A general solution of these equations encounters great difficulties. For this reason we shall restrict our attention to the approximate solutions valid for $n'_1 \ll n_0$, $n'_2 \ll n_0$, i.e., when the conversion efficiency of the excitation radiation to SRS radiation is small. In addition, if we assume $k' \gg s'$ we get

$$-(s'+k')n'_1 + s'n'_2 = -L'n'_1, \quad -s'n'_1 + (s'+k')n'_2 = L'n'_2.$$

After these simplifying assumptions we obtain the photon flux in the "transmission" scheme:

$$n'_1(l) = \frac{Bn_0(1+R)}{M}\left\{\frac{\exp[(ab_2-L')l] - \exp(-Ll)}{L-L'+ab_2} - \frac{R\exp[(ab_2-2L-L')l] - R\exp(-Ll)}{ab_2-L-L'}\right\}, \qquad (34)$$

where $a = An_0e^{-Ll}/M$, $b_2 = (1-R)(1-\gamma_1)$. Consider two typical cases:

1) If $L - L' \ll ab_2 \ll L$ we have

$$n'_1(l) = \frac{B(1+R)}{Ab_2}\{\exp[An_0b_2l\exp(-Ll) + (L-L')l] - 1\}. \qquad (35)$$

The maximum photon number $n'_1(l)$ is achieved at thickness l_{M} which obeys the condition

$$l_{\text{M}} = \frac{1}{L}\left(1 + \frac{L-L'}{An_0b_2}e^{Ll_{\text{M}}}\right). \qquad (36)$$

2) At hyperresonance $L' \ll L$, $ab_2 \ll L$ we have

$$n'_1(l) = \frac{Bn_0(1+R)}{LM}\{\exp[(ab_2-L')l] + R\exp(-2Ll) - (1+R)\exp(-Ll)\}.$$

In this case the optimal layer thickness is determined by

$$l_{\text{opt}} = \frac{1}{L}\left[1 + \frac{(1+R)L}{An_0b_2}\right]. \quad (37)$$

We note that the optimal layer thickness decreases as the excitation intensity increases.

Consider a bulk sample, where we are interested in SRS by a thin, near-surface crystal layer. In this case the opposing fluxes model equations have the form:

$$\frac{dn_1'}{dx} = -L'n_1' + be^{-Lx} + a_1n_1'e^{-Lx}, \quad (38)$$

$$\frac{dn_2'}{dx} = L'n_2' - be^{-Lx} - a_2n_2'e^{-Lx}, \quad (39)$$

where we define

$$a_1 = An_0(1+\gamma_1R), \quad a_2 = An_0(\gamma_1+R), \quad b = Bn_0(1+R).$$

In the "transmission" scheme the photon beam is

$$n_2'(0) = \frac{b}{a_2}\left(\exp\frac{a_2}{L} - 1\right). \quad (40)$$

The depth x_{M} at which the beam n_1' inside the crystal peaks is

$$x_{\text{M}} = \frac{\ln(a_1/L')}{L}. \quad (41)$$

Thus we find that as the excitation intensity increases the position of the peak SRS intensity moves deeper into the crystal. Recall that these relations are only valid if $n_1' \ll n_0$, $n_2' \ll n_0$.

Let us return to equation (39). Letting the multiplier of n_2' in this equation go to zero and setting $x = 0$ we obtain the following formula for the SRS threshold in the "transmission" scheme (bulk sample):

$$(n_0)_{\text{th}} = \frac{L'}{A(\gamma_1+R)}. \quad (42)$$

As resonance is approached, the RS cross-section, which is proportional to A, increases. But the effective absorption coefficient L' increases also, and as a result the SRS threshold decreases only slightly. The hyperresonance case of $L' \ll L$ is an exception. There, the effective absorption coefficient L' remains small in the resonance region, whereas the quantity A increases. Consequently the SRS threshold falls considerably. At the same time, the measured component intensity, proportional to the ratio A/L, remains constant as resonance is approached.

3. RESONANCE CONDITIONS FOR DIFFERENT TYPES OF SCATTERING

It is helpful to consider the resonance conditions for RS and SRS, and to compare these with the hyperresonance conditions for these processes.

A large number of studies have focused on resonant RS spectra, developing the theory of resonant RS and reporting a wide range of experimental data. We shall only quote some recent review articles.[16-18] The theory of resonant HRS is developed in Ref. 19. According to Ref. 17 the following expressions hold for the absorption coefficient k and RS line intensity:

$$k_r = \frac{\pi\omega|\mathbf{eP}_{rk}|^2}{\hbar[(\omega_{rk}-\omega)^2+\Gamma_r^2]}, \quad (43)$$

$$I_{\text{RS}} = \frac{\omega^4 I_0 |S_{nk}|^2_{\text{RS}}}{4\pi c^3\hbar^2}, \quad (44)$$

where

$$(S_{nk})_{\text{RS}} = \sum_r\left[\frac{(\mathbf{eP}_{rk})(\mathbf{e}'\mathbf{P}_{nr})}{\omega_{rk}-\omega+i\Gamma_r} + \frac{(\mathbf{e}'\mathbf{P}_{nr})(\mathbf{eP}_{rk})}{\omega_{rk}+\omega'+i\Gamma_r}\right]. \quad (45)$$

In the above $\mathbf{e}$ and $\mathbf{e}'$ are the unit polarization vectors of the excitation and scattered electromagnetic waves, $\mathbf{P}_{rk}$ and $\mathbf{P}_{nr}$ are the dipole transition matrix elements for the $k \to r$ and $r \to n$ transitions respectively (Fig. 3), and $\hbar\omega_{rk}$ is the energy of electron state r. In Ref. 19 we find a more complicated expression for $(S_{nk})_{\text{HRS}}$ in HRS (transitions involve two intermediate levels r and s):

$$(S_{nk})_{\text{HRS}} = \sum_{r,s}\left[\frac{(\mathbf{eP}_{nr})(\mathbf{e}'\mathbf{P}_{rs})(\mathbf{eP}_{sk})}{(\omega_{sk}-\omega+i\Gamma_s)(\omega_{rn}+\omega'+i\Gamma_r)} + \frac{(\mathbf{eP}_{nr})(\mathbf{eP}_{rs})(\mathbf{e}'\mathbf{P}_{sk})}{(\omega_{sn}+2\omega+i\Gamma_s)(\omega_{rn}+\omega'+i\Gamma_r)} + \frac{(\mathbf{e}'\mathbf{P}_{ns})(\mathbf{eP}_{sr})(\mathbf{eP}_{rk})}{(\omega_{sk}-2\omega+i\Gamma_s)(\omega_{rk}-\omega+i\Gamma_r)}\right]. \quad (46)$$

The RS intensity is resonantly enhanced as $\omega \to \omega_{rk}$, where r is one of the intermediate electron levels of the system. The HRS resonance correspondingly occurs when $2\omega \to \omega_{sk}$. If the $\omega \approx \omega_{rk}$ condition is fulfilled simultaneously, double HRS resonance occurs and the intensity is further enhanced. In Ref. 19 it is estimated that if $\Gamma/2\pi c = 50\ \text{cm}^{-1}$ HRS intensity is enhanced by a factor of 10^6 at resonance and 10^{12} at double resonance.

Unfortunately such optimistic estimates of RS and HRS resonant intensity enhancement are largely illusory, for according to (43) the system absorption also increases as the excitation frequency is tuned towards the resonance. In the simplest and probably most common case, when among the various intermediate levels $r, s, \ldots$ the one that is important in scattering is where the system ends up after absorbing an $\hbar\omega$ photon (RS) or two such photons (HRS), there is a simple connection between scattering and absorption spectra. It follows from (43), (45), and (46) that the scattering cross section and the absorption coefficient are mutually proportional. But then, as we have seen in the preceeding section, given ideal measuring conditions, tuning the excitation frequency towards resonance does not enhance the observed intensity of scattered light. This follows from the fact that if the experimental conditions are propertly selected (the scattering layer thickness, in particular), the RS and HRS intensities in "transmission" and "reflection" schemes are proportional to B/L (RS) or β/L' (HRS), where B and

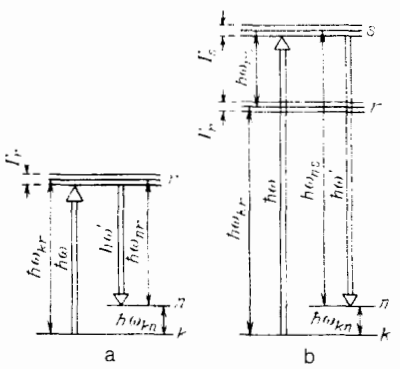

FIG. 3. Stokes transition diagrams in resonant RS (a) and resonant HRS (b).

β are proportional to the scattering cross section, and L, L' are related to the absorption coefficient at frequency ω (RS) or $\omega' = 2\omega \pm \omega_k$ (HRS) by formulae cited in Sec. 2.

The real gain in scattered light intensity achieved by tuning the excitation towards resonance in RS and HRS can occur in two ways.

1) In many cases it is quite difficult to achieve ideal measuring conditions indicated by the opposing fluxes model theory. For example, a sufficiently thick sample of a weakly absorbing crystal or a sufficiently thin strongly absorbing film may not be available. Then a proper choice of excitation frequency makes it possible to approach ideal measuring conditions. Another method, employed in the early work on resonant RS,[20,21] is to dilute solutions of strongly absorbing dyes, leading to reduced absorption but leaving unchanged the scattering layer thickness.

2) In dispersive media with small absorption coefficients k, the parameters L and L' grow more slowly than k as resonance is approached. This also yields a real gain in the scattered light intensity.

Additional intensity gain can be achieved by satisfying the hyperresonance condition. In Fig. 4 we schematically plot the scattered light intensity (proportional to photon flux n_1') against layer thickness l in the "transmission" scheme. Given ideal measuring conditions, according to formulas (18), (23), and (30), the intensity at hyperresonance is enhanced by a factor of e. Let us note that the hyperresonance condition is easy to satisfy in HRLS and HRS measurements.

In the general case, RS line intensity depends on the position of several intermediate levels and there is no simple connection between absorption and Raman scattering. This results in different RS line intensity ratios for lines of different symmetry or lines involving different intermediate levels. Some examples of RS and HRS spectra taken under different excitation conditions are cited below.

4. CRYSTALLINE POWDERS

Thin, plane-parallel layers of crystalline powders can be used as models of experimentally more difficult systems, such as films and near-surface crystal layers. In powders it is easy to change the dispersion of layer thickness and to determine the system parameters L, L', R, R'. This approach was used in Refs. 22–24 to study the behavior of RS and measure the RS cross-sections in dispersive media.

The authors of Ref. 22 used stilbene powder, which has a fairly strong and conveniently measured RS line $\Delta\nu = 1593$ cm^{-1}. Stilbene powder was divided into four fractions of different grain size (Table I). Each powder fraction was loaded into plane-parallel cells of 12 and 30 mm diameter and 1, 2, 3, 4, and 5 mm thickness.

TABLE I. Material parameters for different stilbene powder fractions.

Fraction number	Grain size, mm	L, cm^{-1}	R
1	From 0.1 to 0.2	11.8	0.30
2	From 0.2 to 0.3	11.5	0.25
3	From 0.3 to 0.4	9.9	0.20
4	From 0.4 to 0.5	7.2	0.10

Experimental results were compared with the theory of formula (20), which can be conveniently rewritten as[3)]

$$\frac{n_{10}'}{l} = \frac{I}{l} = \varkappa f(R,\ Ll). \tag{47}$$

Only two variable quantities, R and Ll, enter into (47), together with the scattering coefficient $\varkappa$. The quantity L can be independently determined by measuring the dependence of the excitation line intensity on cell thickness according to (7). Quantities R and Ll were calculated from the measured I/l values at several l, and the dependence $f(R, Ll)$ was calculated for each stilbene fraction. The calculated system parameters L and R are listed in Table I. In Fig. 5 we compare the experimental data (various kinds of points) and calculated curves. The scattering coefficient $\varkappa$ of a given RS line can then be determined from the scattering medium parameters and the calculated $f(R, Ll)$ function. The scattering cross section is then

$$\chi = \frac{\varkappa}{I_0}. \tag{48}$$

Conventional measurements of RS line cross sections require the highest quality transparent crystals of sufficiently large size. For this reason RS cross sections are currently known for only a small number of crystals. Subjecting dispersive absorbing media to similar measurments will significantly extend the range of available systems, as well as enable us to compare the RS cross sections in various states of aggregation, in a wide range of temperatures, in crystals that easily become turbid, and so forth.

As an example, in Table II we cite the measured data on the dependence of the RS cross section on temperature in benzene ($\Delta\nu = 992$ cm^{-1}) and the temperature and state of

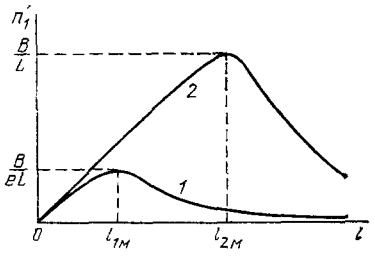

FIG. 4. Dependence of the number of scattered light photons n_1' on scattering layer thickness l in the "transmission" scheme (1—in absence of hyperresonance; 2—at hyperresonance).

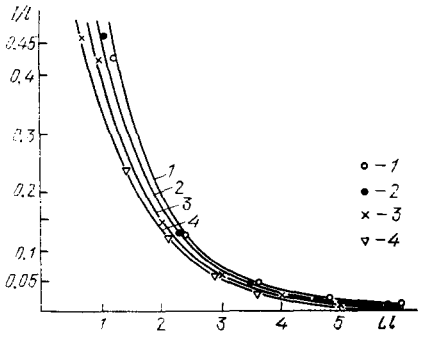

FIG. 5. Experimental (points) and theoretical (curves) dependence of I/l on Ll in different fractions of stilbene powder (1–4 are fraction numbers).

TABLE II. Raman scattering cross sections of benzene and stilbene.

Material	State of aggreg.	Temperature K	$\chi, 10^{-28}$ cm^2
Benzene, $\Delta\nu = 992$cm^{-1}	Solid	101	46
		172	55
		252	55
	Liquid	293	2.05
Stilbene, $\Delta\nu = 1593$ cm^{-1}	Solid	293	460
	Liquid	420	26

aggregation behavior of the RS line in stilbene ($\Delta\nu = 1593$ cm^{-1}).

In these measurements the source was a low pressure mercury lamp ($\lambda = 435.8$ nm line). The light was focused by a lens into a nearly parallel beam directed at a cell containing the power or liquid being studied (sometimes the cell was inside a cryostat). Light scattered into the aperture angle Ω was collected in spectrometer slits. The integrated intensities of the RS line and the excitation line being studied were measured. In the case of liquids and pure single crystals the RS cross section (per molecule) was calculated from the formula

$$\chi = \frac{4\pi I n^2}{I_0 l N \Omega}, \qquad (49)$$

where n is the index of refraction; Ω is the solid angle subtended by the crystal; I_0 is the measured excitation line intensity; N is the number of molecules per unit volume.

There is a notable difference between the RS cross-sections in liquids and crystals (see Table II). This difference is discussed in Ref. 25.

The above technique was also employed in the study of a more complex crystal → liquid crystal → liquid phase transition. The studied materials were 4,4′-azoxyanisole and anisaldazine, excited by the $\lambda = 514.5$ nm line of an Ar laser.

A hollow teflon disk capped with quartz windows at both ends was used to hold the material. The cell was filled with filtered crystalline powder of 0.2–0.3 mm grain size. The 1 mm thickness of the cell was chosen to correspond to ideal RS measurement conditions in the "transmission" scheme [see formula (22)]. Complementary measurements were performed on 1, 2, and 3 mm thick cells in order to calculate the material parameters L and R. Raman scattering spectra of liquid and liquid-crystal phases were measured in the same cells. A detailed description of the measurement techniques is available in Ref. 24. Experimental results are sumamrized in Table III. As in the preceeding case, the RS cross section decreases sharply as the system changes from crystal to liquid. In the liquid crystal the RS cross section is higher than in the liquid, but much lower than in the crystal.

The studied materials belong to the nematic liquid crystal type, characterized by the pronounced elongation of constituent molecules. For example, the 4,4′-azoxyanisole molecule

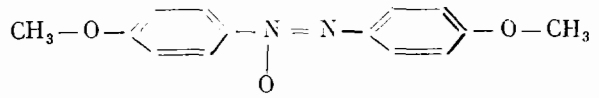

looks, in the first approximation, like a "rod" of 2 nm length and 0.5 nm diameter. During the crystal → liquid crystal transition the long-range order in the location of the molecular centers of gravity is destroyed, whereas the orientation order persists. During the liquid crystal → isotropic liquid transition the long-range molecular orientation order also disappears, but the short-range order remains. The data of Table III indicate the important effect of long-range order in the scattering medium on the RS cross section.

In the solid phase the studied materials are colored powders of bright yellow (4,4′-azoxyanisole) and reddish (anisaldazine) color. They absorb strongly in the blue-green spectral range, which includes the excitation line $\lambda = 514.5$ nm. Therefore the data correspond to resonant (and possibly even hyperresonant) RS excitation. The high measured values of RS cross sections reflect the resonant character of the excitation.

As an example of studies of crystal phase transitions using the HRLS method, consider the data on barium titanate. The most interesting transition in this crystal is the tetragonal (ferroelectric) → cubic (paraelectric) phase transition at $T = 393$ K. In the cubic phase HRLS is forbidden by the selection rules. In the ferroelectric phase the nonlinear susceptiblity tensor components d_{ij} are related to the spontaneous polarization P_s and change with temperature in proportion to P_s.[26] In the paraelectric phase all d_{ij} should equal zero. We note that in Ref. 26 the second harmonic intensity was measured in a single-domain $BaTiO_3$ crystal in the tetragonal modification. Since the crystal becomes multi-domain when heated above 100 °C the actual phase transition region (near 120 °C) was not studied.

The HRLS intensity in a wider temperature range was studied in Refs. 27, 28. The source was a Nd^{3+}:YAG laser (generation line $\lambda = 1.06\,\mu$m). Laser radiation was directed into the cell containing barium titanate powder of ~1 mm grain size. The cell consisted of two quartz windows enclosing a 0.3 mm thick layer of barium titanate powder. The cell was placed inside a heater (details of the experimental method are described in Refs. 27, 28).

TABLE III. Raman scattering cross sections of liquid, liquid crystal, and crystal states.

4,4′-azoxyanisole, $\Delta\nu = 904$ cm^{-1}			Anisaldazine, $\Delta\nu = 1003$ cm^{-1}		
t, °C	State of aggreg.	χ, 10^{-28} cm^2	t, °C	State of aggreg.	χ, 10^{-28} cm^2
25	Crystal	200	25	Crystal	950
144	"	240	165	"	1400
125	Liquid crystal	11.4	173	Liquid crystal	110
140	Liquid	5.7	185	Liquid	41

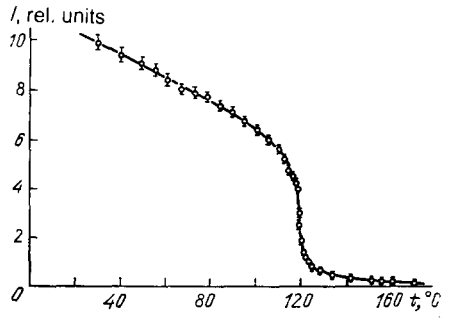

FIG. 6. Temperature dependence of HRLS intensity in barium titanate powder,[27,28]

The experiments were carried out in the "reflection" scheme. The measured temperature dependence of the HRLS line intensity is represented in Fig. 6. It is clear that the HRLS intensity decreases as the sample is heated and falls sharply near the phase transition (120 °C). Even after the phase transition HRLS intensity does not fall to zero, which probably indicates deviation from cubic symmetry in some regions of the high-temperature barium titanate phase. Similar deviation from selection rules after the phase transition was also observed in the RS spectra.[29]

In the first approximation I_{HRLS} in the ferroelectric phase goes as the square of the nonlinear suceptibility tensor components d_{ij} and therefore as the square of the spontaneous polarization P_s. In the tetragonal phase the relation $I_{\text{HRLS}} = AP_s^2$ holds (see Ref. 27). Consequently the temperature dependence of I_{HRLS} in ferroelecric crystals sheds light on the changes in their dielectric properties.

The low-temperature phase transitions of barium titanate were also studied by this method. The results are plotted in Fig. 7 in conjunction with the data on spontaneous polarization.[30] The change in I_{HRLS} near 273 K accompanied by a well-defined hysteresis is quite evident, as is the phase transition near $T = 190$ K. In the low-temperature phases of barium titanate a decreasing spontaneous polarization P_s corresponds to an increase in HRLS intensity, which may be explained by changes in the nonlinear susceptibility tensor because of the tetragonal→rhombic crystal phase transition.

In this way the temperature dependence of HRLS makes it possible to track crystal phase transitions from one noncentrosymmetric modification to another.

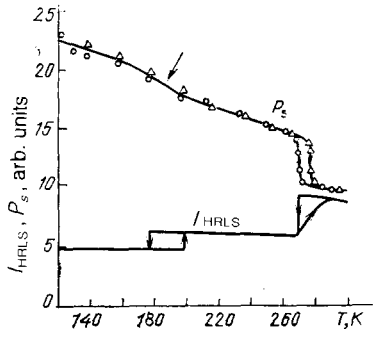

FIG. 7. Temperature dependence of I_{HRLS} and spontaneous polarization P_s in barium titanate crystals.[30]

Stimulated Raman scattering in crystalline powders was first observed by Zubov and co-workers.[1] Subsequently, a large number of studies addresed this phenomenon.[2-4,7-11] The possibility of studying SRS in dispersive media has considerably expanded the range of available systems. Stimulated Raman scattering in deeply cooled and frozen liquids, and molecular crystals, has been investigated in the above studies and in Refs. 31–35. Resonant SRS has also been examined.[6,36] We note that the authors of Ref. 35 have observed low-frequency SRS lines in the 20–100 cm^{-1} range, corresponding to crystalline lattice vibrations.

Most of the research into the variation of SRS line intensity with experimental parameters has been carried out on stilbene crystals ($\Delta\nu = 1593\ \text{cm}^{-1}$). Here we cite some of the results obtained in conditions of low SRS conversion efficiency.

The dependence of the stilbene line intensity on the thickness of the crystalline powder layer was studied in Ref. 3. The measured curves clearly indicate the peak intensity conditions (Fig. 8, a). The dependence of the layer thickness l_{M}, which maximizes the energy of the first SRS Stokes component, on the excitation energy E_0 is illustrated in Fig. 8, b. The solid curve is obtained from formula (36) with the value $L = 10.0$ taken from Table I. The parameter $(L - L')/Ab_2$ which enters into (36) was taken as 0.0315. Taking into account the approximate nature of formula (36) and possible experimental error the agreement of experimental data with calculations is adequate.

The above results were obtained with ruby laser excitation ($\lambda = 694.3$ nm) of SRS. References 36, 37 reported the use of this laser's second harmonic ($\lambda = 347.1$ nm). In this case the excitation line falls into the region of the long-wavelength absorption tail and experiences a fairly high absorption coefficient $k = 12.5\ \text{cm}^{-1}$, whereas the absorption coefficient for the first Stokes component of SRS $\Delta\nu = 1593\ \text{cm}^{-1}$ is much lower (Fig. 9). Consequently, the hyperresonance condition is fulfilled. The authors of these studies remarked on the relatively weak inensity of the studied SRS line. The intensity of the SRS line excited by the laser second harmonic was not appreciably different from its countrpart excited by the fundamental ($\lambda = 694.3$ nm), although the expected gain in the RS cross section was a factor of 10^4. Absorption of excitation radiation by stilbene was cited as the factor preventing resonant SRS generation. This conclusion agrees with the estimates of Sec. 3.

5. FILMS

Metallic and semiconducting films on various substrates play an important role in modern technology. The study of film structure and properties by light scattering methods is consequently of great interest. In practice most modern microcircuits are built on silicon crystal surfaces. Accordingly a major research area in very large scale integration of electronic devices is the production of submicron silicon layers and films with controlled properties, the study of their structure and its evolution in the course of technological processing.

Raman spectra of epitaxial films grown on crystalline substrates were investigated in Refs. 38–47. One of the experimental conclusions was that RS lines in films are shifted in frequency from their positions in single crystals. The halfwidth and intensity of these lines were also measured.

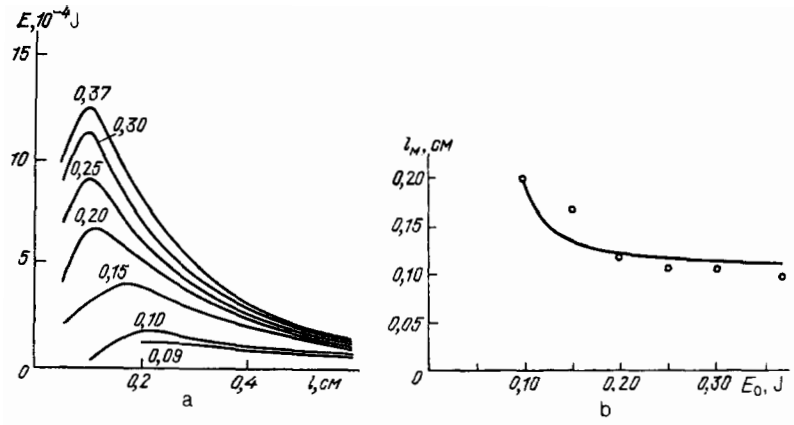

FIG. 8. a—Effect of sample thickness on the energy of the first SRS Stokes component in stilbene powder; numbers indicate the excitation radiation energy E_0 (in J).[3] b—Dependence of optimal powder layer thickness l_M on excitation radiation energy.

Raman scattering in silicon films has been studied by argon laser ($\lambda = 488.0$ nm) and copper vapor laser ($\lambda = 510.6$ nm) excitation.[41,42] According to Ref. 44 data on the absorption spectrum of silicon, these sources should satisfy the hyperresonant RS condition. The results are plotted in Fig. 10.

In the silicon single crystal spectrum there is an RS line due to the triple degenerate sublattice vibrations at frequency 521 ± 0.3 cm^{-1}. In the spectrum of an $l = 0.31$ μm thick silicon film on a gallium phosphide substrate this line is frequency-shifted by 5.6 cm^{-1} towards lower frequencies. In films on other substrates RS lines are shifted towards higher frequencies. The smallest frequency shift of 1.6 ± 0.3 cm^{-1} is observed in a silicon film (thickness $l = 1.0$ μm) on a germanium substrate. The shifts for silicon films on spinel ($l = 0.8$ μm), on sapphire in the $[\bar{1}012]$ orientation ($l = 0.60$ μm) and in the $[10\bar{1}2]$ orientation ($l = 0.44$ μm) are 2.4, 3.1, and 4.0 cm^{-1} respectively.

According to the theory,[38,47] RS line frequency shifts in silicon films are due to the stresses which are created in the films as they are cooled from growth to room temperature. When a film sample (or a single crystal) is heated the RS lines are shifted in frequency and the frequency difference between the two shrinks. At growth temperatures the frequency difference disappears.

The intensity I_{RS} of the RS line in thin silicon films is proportional to their thickness l. As l increases the intensity increases, in agreement with formula (15), saturating at the silicon single crystal value. In Fig. 11 we compare the calculated dependence from expressions (21) (with $L = L'$) and (15) (with $L \neq L'$) with experimental results of Refs. 42, 45. Reference 44 on the optical parameters of silicon furnished the computational parameters $L = 1.43 \cdot 10^4$, $L' = 1.19 \cdot 10^4$, $R = R' = 0.38$. Clearly, even though the difference between L and L' is small, the "hyperresonance" formula is in better agreement with experimental data than formula (21) which neglects the difference between L and L'.

The observed dependence of RS line intensity on film thickness provides a new method of measuring the thickness of submicron films.[42,45] The "reflection" scheme is used: the laser beam is alternately directed at the studied film and a calibration film. In each case the RS line intensity is measured. Then the thickness of the examined film is established from a comparison with a calibrated plot of RS line intensity as a function of film thickness. This method can be used to measure the thickness of different films on different substrates.[4)]

Scattered light spectra reflect the evolution of near-surface layers in single crystals and films that are subjected to ion implantation, laser and thermal annealing, or other technological operations employed in modern semiconductor technology.

Silicon films of 0.6 μm thickness on sapphire substrates have been irradiated by giant laser pulses (ruby laser, 100 MW power).[42,45] After irradiation the RS spectrum con-

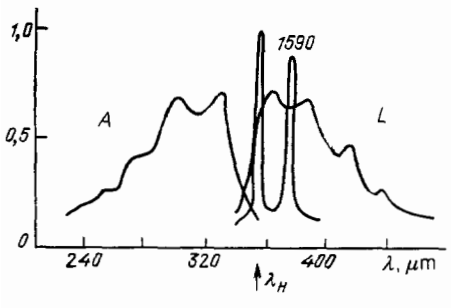

FIG. 9. Absorption (A) and luminescence (L) spectra and SRS in polycrystalline stilbene.[36,37] (Arrow marks the excitation wavelength, SRS frequency is indicated above its line).

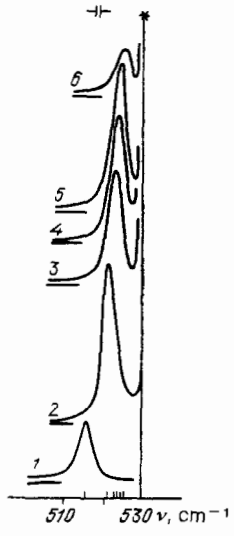

FIG. 10. Spectra of silicon single crystal (curve 2) and silicon films on substrates:[41,42] 1—gallium phosphide; 3—germanium; 4—spinel; 5—sapphire in the $[\bar{1}012]$ orientation; 6—sapphire in the $[10\bar{1}2]$ orientation. Argon laser discharge line is marked with an asterisk.

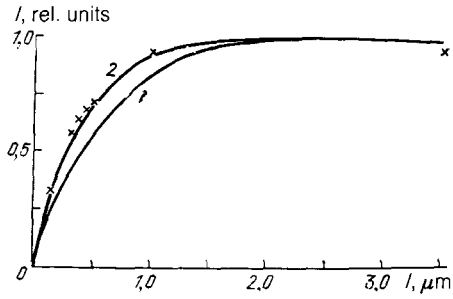

FIG. 11. Dependence of RS line intensity I on thickness l of silicon film on a sapphire substrate: 1—calculated from (21) with $L \neq L'$; 2—calculated from (15) with $L \neq L'$. Points are experimental data of Ref. 45. Argon laser 488.0 nm line was used to excite the 521 cm^{-1} line of silicon.

tained two lines. One matched the frequency of unirradiated films, the other was shifted towards lower frequencies.

Laser irradiation produced a spot on the sample surface with uneven fluence distribution over its area. In order to register the RS spectra of different areas in this spot the sample was placed in a special holder and scanned across the RS excitation laser beam. The spectra of different regions (each 0.15×1.5 mm^2 in area) are plotted in Fig. 12. It is evident that near the center of the irradiated spot the RS line frequency is broadened and lowered in frequency.

The low-frequency tails of spectra 3–5 exhibit additional maxima. In the spectrum of region 5 (the center of the irradiated spot) the additional maximum is at 519.1 cm^{-1} and the full linewidth is 9.6 cm^{-1}.

Observed changes in RS spectra can be explained as follows. Laser irradiation of 1 J/cm^2 fluence melts the near-surface layer of the silicon film to a depth of about 0.2 μm depth. At the depth of 0.4 μm the film layer is in immediate contact with the substrate and remains crystalline. After irradiation the sample quickly cools and recrystallizes. The thin silicon layer in contact with the substrate contributes the intensity peak that matches the line from an unirradiated

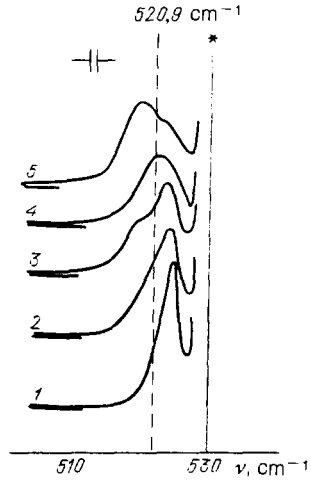

FIG. 12. Raman spectra of different areas on the surface of a silicon film on sapphire after laser irradition[42,45]: 1—unirradiated region; 2—border of the irradiated region; 3—near the border (inside the irradiated region); 4—near the center of the irradiated region; 5— center of the irradiated region. The dashed vertical line corresponds to the silicon single crystal frequency. Argon discharge line is marked with an asterisk.

film on a sapphire substrate. The upper, recrystallized film layer is expanded to a lower density and contributes the frequency-shifted RS line.

We remark that the success of these experiments is due to the possibility of registering RS spectra from silicon layers at a depth of 0.5–0.6 μm from the surface.

By this method is is possible to reconstruct the inhomogeneity distribution on the film surface from the parameters of the RS lines. Yet another, more effective means of studying film inhomogeneities is the HRLS method. According to Ref. 48, HRLS intensity is proportional to $|\chi^{nl}|^2$, where χ^{nl} is the nonlinear susceptibility of the crystal. In isotropic media, made up of molecules with inversion centers, $\chi^{nl} = 0$, i.e, HRLS is forbidden. Accordingly, when a sample in which regions of forbidden HRLS alternate with HRLS-permitted ones is scanned across the excitation beam, the HRLS intensity exhibits sharp jumps.

As an example, Fig. 13 illustrates the scanning of two samples across a laser beam. The films under study were: a slant cleaved 78 μm thick $GaP_{0.84}As_{0.16}$ film on a gallium phosphide substrate, and a 1.0 μm thick AlN film on sapphire. The 578.2 nm line of a copper vapor laser was used for HRLS excitation in the "reflection" scheme. The HRLS wavelength was 289.1 nm, falling into the strong absorption regions of both films.

We see from Fig. 13, a (region a–b) that as we pass from the free substrate surface to the film the HRLS intensity is markedly reduced.[5)] In the slant cleaved region of the film (b–c) HRLS intensity oscillates more than in the flat region (c–d), since the b–c region of the film was polished mechanically. The thin AlN film (Fig. 13, b) exhibits even greater inhomogeneity, as evidenced by the HRLS intensity oscillations.

6. SINGLE CRYSTALS

Many experimental and theoretical papers, as well as several review articles, have examined resonant RS in single crystals.[6,49–53] In some cases the hyperresonance conditions were also satisfied. It is helpful to analyze the results obtained in these studies within the theoretical framework developed in Secs. 1 and 2.

First, let us consider the peculiar RS spectra of cadmium sulfide. The bandgap of this crystal is 2.6 eV, which corresponds to a 452.1 nm wavelength. Therefore, when RS is excited by a 488.0 nm (that is, 2.39 eV) argon laser line on the hyperresonance condition is fulfilled, despite the low frequency of RS lines: 232 cm^{-1} (A_1, TO) 301 cm^{-1} (A_1, LO), 240 cm^{-1} (E_1,TO), 307 cm^{-1} (E_1, LO).

Indeed, changing from the 480.0 nm to the 496.5 nm Ar laser line, i.e., changing the frequency by 340 cm^{-1}, changes the absorption coefficient k from 24 cm^{-1} to 5.8 cm^{-1} at 6 K.[54] At room temperature $k \approx 10^4$ cm^{-1} for the 488.0 cm^{-1} line.[6)]

Several "anomalies" in the resonant CdS spectra were noted in Refs. 54–58. It turns out that the RS lines based on LO-phonons—ostensibly forbidden by selection rules—have high intensities in these spectra. As the excitation frequency is tuned towards the bandgap the forbidden line intensity increases sharply. For example, in the $x(zz)y$ geometry[54] the forbidden LO-phonon RS line manifests itself as a barely discernible peak on a broad band at 514.5 nm excitation, but 488.0 nm excitation produces a sharp, intense peak.

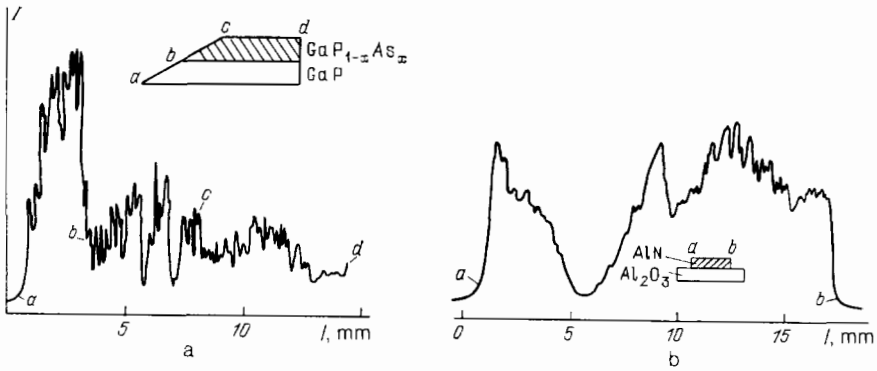

FIG. 13. Hyper-Rayleigh scattering by thin film surfaces.[45] a—$GaP_{1-x}As_x$ film on gallium phosphide. b—AlN film on sapphire. Insets show film structures.

Systematic studies of Raman scattering in CdS at 77 K (sample placed in liquid nitrogen) and 300 K were reported in Refs. 54–57. An Ar laser beam was incident at 5° from the surface of a polished edge in the sample crystal. Measurements were taken on the same side of the crystal at right angles to the incident beam.[55,56] In Refs. 54, 57, 58 the "reflection" scheme was used. The focus of Ref. 57 was the different behavior of LO- and TO-phonon RS cross sections as the absorption band was approached. When photon energy was raised from 1.7 to 2.2 eV the A_1 and E_1 symmetry TO-phonon cross sections fell to zero; at higher energies they increased sharply. In contrast, the LO-phonon cross sections increased monotonically through the resonance. The authors explained this effect by the interference of nonresonance terms with the resonance term in the scattering formula. The dependence of RS intensity on phonon wavevector $\mathbf{k}$ was studied in Refs. 58, 59. The most interesting feature was the comparison of RS spectra taken at $\mathbf{k}_{min}$ and $\mathbf{k}_{max}$. To this end, spectra of 0° and 180° scattering (all other conditions being equal) were juxtaposed in Ref. 59, whence it was deduced that LO-phonon RS intensity increased with $\mathbf{k}$.

Interesting results were reported in Ref. 56. The authors excited the CdS RS spectrum by the 457.9 nm line. Up to nine replica LO oscillation lines were observed (Fig. 14). Analogous results were obtained for a number of other crystals (Table IV).

The oscillation frequency of LO replicas are proportional to the replica number with high precision. Their linewidth is narrow, in contrast to the usual higher harmonics of RS spectra taken far from resonance. This same behavior is exhibited by resonant RS spectra of several other crystals, as well as diphenylpolyenes[21] and iodine solutions. These spectra are superficially similar to SRS spectra, characterized by the large number of Stokes components with narrow linewidth and frequencies strictly proportional to the component number.[60] As an example, Fig. 15 presents the SRS spectrum of sulfur,[11] which contains 8 components. The theory of crystal RS spectra in the resonance region is discussed in Ref. 53.

The hyper-Raman effect was also observed in the CdS crystal.[61–63] These spectra were excited using the Nd^{3+}:YAG laser ($\lambda = 1064$ nm) operating in the Q-switched regime. The $z(y, z+y)x$ geometry was employed in order to exclude the two-step process of second harmonic generation followed by RS excitation at frequency 2ω. In this geometry the excitation radiation is directed along the optic crystal axis (z axis), second harmonic generation is forbidden and two-step processes are excluded. Scattered light was measured in directions perpendicular to the excitation propagation.

In order to reach the resonance condition the crystal was heated to shrink the bandgap.[61] The authors studied resonance HRS based on longitudinal optical phonons E_1 (LO) of 307 cm^{-1} frequency. They discovered that the intensity of both the Stokes and the anti-Stokes HRS components first increased with temperature and then fell abruptly. The authors explained this sharp decrease by absorption of scattered light within the crystal. The observed HRS intensity enhancement by a factor of approximately three as the temperature was raised from 150 to 350 K is in good agreement with the estimates of Sec. 2, which predict HRS intensity enhancement by a factor of $e = 2.71$ when resonant spectrum excitation is replaced by hyperresonant excitation.

Nonlinear $LiNbO_3$ and $LiTaO_3$ crystals are of great interest when it comes to comparing the spectra produced by different types of scattering. These crystals are widely used in nonlinear optics, particularly for laser frequency conversion—for this reason they were exhaustively investigated in a number of studies.[64–71]

The vibrational spectrum of lithium niobate and tantalate has the form:

$$\Gamma = 4A_1\ (\text{IR, RS, HRS}) + 5A_2\ (\text{HRS}) + 9E\ (\text{IR, RS, HRS}).$$

Vibrations are split into TO- and LO-components. In the lithium niobate RS spectrum in the $y(zzx)y$ geometry A_1 (TO) oscillations are allowed: at 300 K the most intense lines are $1A_1$ (258 cm^{-1}), $2A_1$ (281 cm^{-1}), and $4A_1$ (639 cm^{-1}).[71] In the $x(yz)x$ geometry E (TO) oscillations are allowed: the most intense lines are 1E (155 cm^{-1}), 2E (239 cm^{-1}), and 7E (584 cm^{-1}). In the $x(yy)x$ geometry A_1 (TO) and E (TO) oscillations are allowed; in the $y(xx)y$ geometry A_1 (TO) and E (LO) oscillations are allowed; in the $z(xx)z$ geometry A_1 (Lo) and E (TO) oscillations are

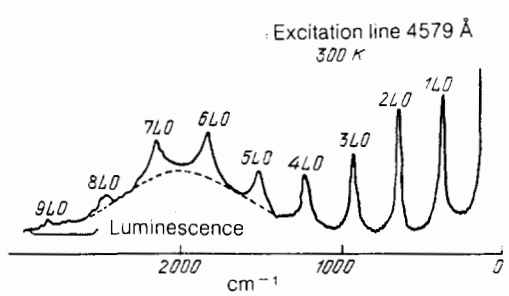

FIG. 14. Cadmium sulfide spectrum at 300 K excited by a 457.9 nm line.[56]

TABLE IV. Raman scattering LO-phonon frequencies (in cm^{-1}) in crystals (data from Ref. 52, p. 561).

LO-component number	Crystal					
	CdS	GaP	ZnTe	ZnSe	InAs	ZnO
1	302—306	403	210	253	241	585
2	607	805	421	506	483	1165
3	910	1208	632	759	730	1749
4	1214		843	1009		2343
5	1520		1055	1267		2928
6	1819					3520
7	2118					4101
8	2417					4678
9	2716					

allowed. Among the LO-phonons the most intense RS lines are 874 cm^{-1} (A_1) and 880 cm^{-1} (E); 282 cm^{-1} (A_1) and 338 cm^{-1} (E) lines are less intense but still quite prominent.

According to the data of Refs. 65, 71 the most intense lines in the RS spectrum of lithium tantalate are A_1 (TO) with frequencies of 186 cm^{-1}, 202 cm^{-1}, and 594 cm^{-1}, and the E (TO) line at 141 cm^{-1}. All LO-phonon lines are weak.

Now let us turn to the HRS spectra. When the 1064 nm line of he Nd^{3+}:YAG laser was employed in the accumulation scheme to excite HRS in lithium niobate it turned out that the most intense lines are: 151 cm^{-1}–E (TO), 784 cm^{-1}–E (TO), and 880^{-1}–E (LO). In the HRS spectrum the 258 cm^{-1}–A_1 (TO) line is of medium intensity. According to Ref. 71 the following lines are quite intense in the HRS spectrum of lithium tantalate: 202 cm^{-1}—A_1 (TO), 594 cm^{-1}–E (TO), and 141 cm^{-1}–E (TO).

A copper vapor laser (578.2 nm line, second optical harmonic $\lambda = 298.1$ nm) was also used to excite HRS in lithium tantalate.[64] HRS data were taken in the continuous registration regime. The use of this laser, which works in the quasicontinuous regime with fairly low pulse power (20 kW), and of a relatively simple data-taking system was successful because of several factors. One of these was the nearly resonant character of HRS excitation. This conclusion is corroborated by the fact that attempts to excite HRS in lithium niobate, which has amore distant absorption band, proved unsuccessful. The "reflection" scheme employed in Ref. 64 was also more effective than the 90° observation geometry commonly used in HRS experiments.

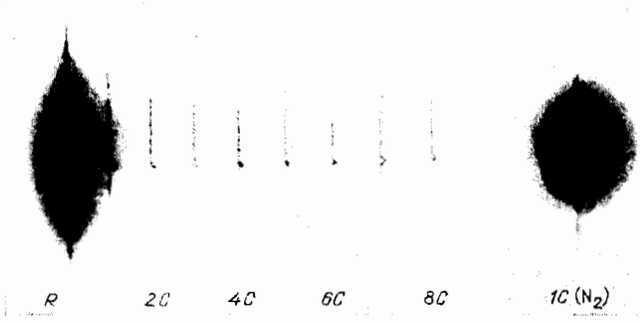

FIG. 15. SRS spectrum of sulfur powder in liquid nitrogen.[11] 1–8—SRS Stokes component series in sulfur; $1C(N_2)$ is the liquid nitrogen component; R is the excitation line.

The following intense lines were observed in the HRS spectrum of lithium tantalate:[64] 202 cm^{-1} and 594 cm^{-1} A_1 (TO) lines; a 355 cm^{-1} line which corresponds to a very weak A_1 (TO) in the RS spectrum; and a 126 cm^{-1} line which corresponds to an intense 141 cm^{-1}–E (TO) line in the RS spectrum. Another interesting HRS line had a frequency ~930 cm^{-1}: this line has no counterpart in the RS spectrum and can be grouped with the "silent" A_2 type modes.

These data demonstrate that the relative intensity of RS and HRS lines can vary significantly. This behavior of the HRS spectra can be explained by the difference in RS and HRS scattering tensors. In lithium niobate E type lines dominate the HRS spectrum, whereas in the RS spectrum A_1 type lines are more intense. This tendency is not as pronounced in lithium tantalate, however.

The SRS phenomenon in lithium niobate and tantalate crystals was studied in greatest detail using ruby laser excitation at 694.3 nm.[70] The measurements were taken at 300 K. Laser radiation was focused onto the crystal in a parallel beam with the crystal inside a resonator; outisde the resonator a weakly convergent beam was used. In the latter case some vibrational frequencies were shifted slightly because SRS was due to polaritons and propagated at a slight angle to the excitation beam.

In $LiNbO_3$ SRS was observed on $1A_1$ (258 cm^{-1}), and $4A_1$ (639 cm^{-1}) TO-phonons when the excitation propagated along the x or y crystal axes. When z axis excitation was used, LO-components of these oscillations—$1A_1$ (282 cm^{-1}) and $4A_1$ (874 cm^{-1})—were excited. These data imply a significant difference in the excitation thresholds of SRS on LO- and TO-phonons. Moreover, they support the general rule that SRS lines are largely produced by fully symmetric vibrations,[17] usually the most intense one in the RS spectrum.

We see that all types of light scattering described in Secs. 2 and 3 have been observed in $LiNbO_3$ and $LiTaO_3$ crystals.

7. NEAR-SURFACE CRYSTAL LAYERS

Near-surface crystal layers are the most difficult to study by light scattering methods and the results of such studies are difficut to interpret because the state of the layer and the effective interaction depth l_{int} of light with the layer are unknown. Often it is assumed that $l_{int} = 1/k$, where k is the absorption coefficient. We have seen earlier, however, that this estimate can be seriously in error. In particular, l_{int}

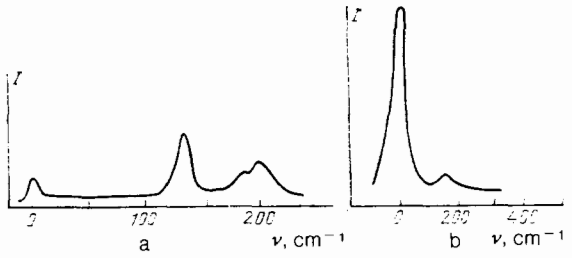

FIG. 16. HRLS and HRS in KCl crystals.[64,71,72] a—Observation at 90° to the incident beam; b—"Reflection" scheme.

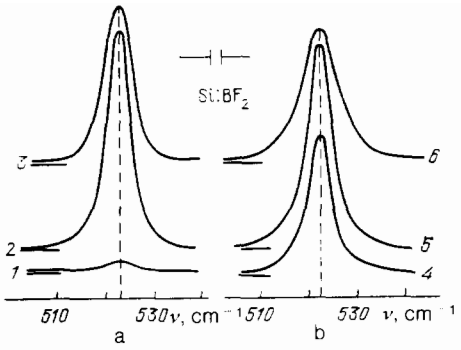

FIG. 17. Raman scattering spectra of silicon implanted with boron fluoride ions of 50 keV (a) and 150 keV energy (b)[42,45]: 1—unannealed sample; 2–6—samples annealed at 1000 °C. Implantation doses: 1, 2, 4—$6.3\cdot10^{14}$ cm^{-1}; 5—$12.5\cdot10^{14}$ cm^{-1}; 3,6—$31.3\cdot10^{14}$ cm^{-1}.

can be markedly enhanced at hyperresonance.

The near-surface crystal layer is usually inhomogeneous. Even in the absence of extrinsic impurities the crystalline structure is deformed, leading to modification of scattering spectra. To illustrate this, Fig. 16 contains the HRLS and HRS spectra of the KCl crystal taken in different ways. In Fig. 16, a the single crystal spectrum is plotted, with the scattered light registered at 90° to the propagation direction of the exciting beam (data from Refs. 71, 72). Selection rules disallow HRLS in KCl crystals and consequently the observed HRLS signal is due to structural inhomogeneities. The small intensity of the HRLS signal compared to the HRS (144 cm^{-1} line) indicates that in this crystal lattice deformation in the bulk are relatively slight. The situation is quite different when light is scattered by the crystal surface. The spectrum obtained in the "reflection" scheme (Ref. 64) exhibits a much stronger HRLS line (Fig. 16, b). This indicates the deformation of the crystalline structure in the near-surface layer.

Scattering spectra of near-surface layers allow us to study the various processes occurring in these layers during technological processing. Raman spectra of silicon near-surface layers were reported in Refs. 42, 45: these layers were subjected to ion implantation with subsequent laser or thermal annealing. Different doses of arsenic, phosphorus, and boron ions, as well as molecular boron fluoride ions, were implanted at energies from 50 to 150 keV. The thickness of deformed layers in silicon varied between 0.03 and 0.1 μm. Spectra were excited by the 510.6 nm line of a copper vapor laser. As mentioned in Sec. 4 this arrangement fulfills the hyperresonance conditions for RS in silicon.

Silicon single crystal RS spectra contain a 521 ± 0.3 cm^{-1} line with 3.6 cm^{-1} half-width. The frequency of this line is unchanged by implantation, but the line becomes broader and its intensity decreases at higher doses. This behavior is much more pronounced in arsenic implantation than in boron implantation: arsenic ions have greater volume and cause greater deformation of the crystalline lattice in the near-surface silicon layers than the smaller boron ions. After thermal annealing the intensity of this silicon line is enhanced, indicating that the lattice is reconstituted; the frequency remains unchanged from the single crystal value.

For illustrative purposes we plot in Fig. 17 data on the evolution of silicon RS spectra in the course of boron fluoride ion implantation followed by annealing at 1000 °C.[42,45] The molecular boron fluoride ion has an intermediate effect: it is smaller than arsenic but larger than boron. Clearly the line intensity in the unannealed silicon sample is quite low. Annealing restores the intensity given moderate implantation doses, but the lineshape is broadened. Increasing the ion energy decreases the intensity somewhat and further broadens the lineshape.

Laser annealing of implanted silicon samples leads to more complicated changes in RS spectra. The line acquires an asymmetric doublet structure with the asymmetry dependent on the annealing regime. The additional RS line after annealing was first reported in Ref. 73, where silicon single crystals were implanted with silicon ions. Silicon crystals in the [111] orientation implanted with a $43.8\cdot10^{14}$ cm^{-2} dose of 50 keV phosphorus ions or a $62.5\cdot10^{14}$ cm^{-2} dose of 75 keV arsenic ions were studied in Refs. 42, 45. A YAG Laser ($\lambda = 532$ nm) was employed for annealing.

After the silicon single crystal was implanted with arsenic the silicon line disappeared indicating that the near-surface layer was rendered fully amorphous. After the subsequent laser annealing a broad band appeared in the spectrum. The band had two peaks: the main peak at 531 ± 0.3 cm^{-1} and an additional peak at 514.8 ± 0.3 cm^{-1}. As the annealing laser fluence was increased the RS lines became more intense and their asymmetry was reduced. Analogous behavior was observed in silicon implanted with phosphorus. These samples were also subjected to combined annealing: first laser and then thermal. It was observed that the additional line disappeared after combined annealing. The main line had the same characteristics as in the original single crystal, indicating that the crystalline lattice in the near-surface layer was restored.

A significant shift in RS lines of n-Si samples after P, As, or Sb ion implantation followed by laser annealing was observed in Ref. 43. The energies of P, As, and Sb ions were 190, 100, and 350 keV respectively. Frequency shifts as large as 11 cm^{-1} were observed. This study demonstrated that the frequency shift depends on the free carrier concentration. After taking into account changes in the lattice constant, it was shown that experimental data are in good agreement with a model in which virtual transitions of free electrons between Δ_1 and Δ_2 conduction bands are induced by phonons.

In addition to providing a diagnostic tool for technological processing of crystal surfaces, RS spectra can be used to solve general problems in the physics of solid state surfaces.

One such problem is the detection and measurement of surface phonons. This problem is quite difficult because the RS lines corresponding to surface phonons are of low intensity, while their frequencies are only slightly shifted from the more intense bulk phonon RS lines.[74] To date RS methods have only been successful in the study of surface phonons in thin film samples grown on crystalline substrates.[75] Surface phonon states in bulk samples generally differ from their counterparts in thin films,[74] increasing the physical interest of this problem.

A $5\times5\times10\ \text{mm}^3$ gallium phosphide crystal was used in Ref. 76 to study Raman scattering from the [111] plane, where the intensity of bulk longitudinal (LO) phonon lines is markedly lower than from the [100] plane. This improves the possibility of observing surface phonons. In order to avoid sample heating the laser beam was focused onto the sample as an elongated spot. The authors used the 510.6 nm line of a copper vapor laser, which falls into the absorption band of GaP. Consequently the excitation beam did not penetrate more than 20–30 μm into the bulk, enhancing the role of surface effects.

The observed RS spectra are presented in Fig. 18. Two intense lines in the spectra correspond to bulk LO- and TO-phonons. At $T = 100$ K in air the low frequency tail of the LO-phonon peak exhibits only a small asymmetric feature (marked with an arrow on Fig. 18, 1). If the crystal is placed in liquid nitrogen the frequency of this feature is shifted more (Fig. 18, 2) because of the dependence of surface phonon frequency on the permittivity of the medium in contact with the surface. In this case the frequency difference between bulk and surface LO-phonons can be calculated as 4.5 cm^{-1}, while the observed LO-phonon line is 1.8 cm^{-1} wide. The ratio of the surface phonon scattering intensity to the TO-phonon line intensity is $6\cdot10^{-3}$.

More favorable conditions for the observation of surface phonon effects can be created by using crystalline powders, since this increases the total surface area. A gallium phosphide powder with ~1 μm grain size was examined in Ref. 76. RS spectra of this powder in liquid nitrogen and in CCl_4 at 78 K are shown in Fig. 18, 3–4. Clearly the additional peak corresponding to the surface phonon is quite prominent in this case. Analogous results were obtained using ZnSe and CdS powders of smaller than 0.1 μm grain size.

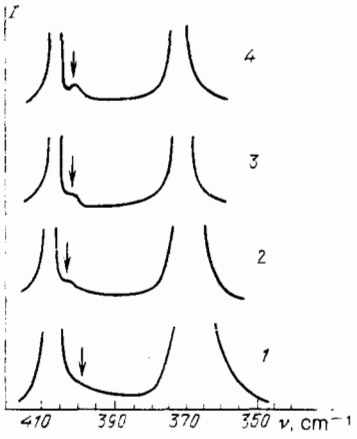

FIG. 18. Raman scattering spectra of gallium phosphide.[76] 1—single crystal at 100 K inside a cryostat; 2—single crystal in liquid nitrogen; 3—powder in liquid nitrogen; 4—powder in CCl_4 at liquid nitorgen temperature. Arrows mark the peak intensities of surface phonon components.

8. CONCLUSION

The experimental material discussed above demonstrates that various types of inelastic light scattering can be successfully employed to solve varied physical and applied problems. The dispersive character of the scattering medium and the associated absorption prove no hindrance to the observation and investigation of scattering processes. An appropriate selection of experimental conditions makes it possible to measure full scattering spectra. An analysis of the resonance excitation conditions indicates that if the absorption at excitation and scattered frequencies is significantly different (hyperresonance) interesting scattering peculiarities come to light. Despite the approximate character of the "opposing fluxes model," this general approach to light scattering in dispersive media holds promise of determining the general tendencies and interrelations among the various types of scattering.

Especially interesting is the successful application of the methods discussed to the study of near-surface layers in crystals and thin films.

[1)]HRLS and SHG also differ in an essential manner in the angular distribution of the frequency-shifted radiation.
[2)]These characteristics of a dispersive medium were introduced by Schuster[13] and later adopted by Gershun.[14]
[3)]This formula neglects reflection from the plates that contain the crystalline powder layer. It is a simple matter, in principle, to include the small corrections due to this change in boundary conditions, but the formulas become significantly more complex.
[4)]Crystal lattice inhomogeneities and strains in the films can distort the intensity of a studied line.[47] According to available data, however, such distortions are unimportant in measuring film thickness by this method.
[5)]In this case both film and substrate are noncentrosymmetric, but their nonlinear susceptibilities are different.
[6)]The significant changes in the absorption coefficient with temperature are due to changes in the bandgap.
[7)]Frequencies and experimental geometries taken from Ref. 66.

[1]V. A. Zubov, G. V. Peregudov, M. M. Sushchinskiĭ, Va. A. Cherkov, and I. K. Shuvalov, Pis'ma Zh. Eksp. Teor. Fiz. **5**, 188 (1967) [JETP LETT. **5**, 150 (1967)].
[2]V. A. Zubov, A. V. Kraiskiĭ, and M. M. Sushchinskiĭ, Energy Distribution in Stimulated Raman Scattering Specta of Dispersive Media, Preprint No. 189 Fiz. Inst. Akad. Nauk SSSR, M., 1968.
[3]V. A. Zubov, A. V. Kraiskiĭ, and M. M. Sushchinskiĭ, Effect of Excitation Parameters on Stimulated Raman Scattering Characteristics of Dispersive Media, Preprint No. 145 Fiz. Inst. Akad. Nauk SSSR, M., 1970.
[4]V. A. Zubov, A. V. Kraiskiĭ, K. A. Prokhorov, M. M. Sushchinskiĭ, and I. K. Shuvalov, Zh. Eksp. Teor. Fiz. **55**, 443 (1968) [Sov. Phys. JETP **28**, 231 (1969)].
[5]I. B. Grun, A. K. McQuillan, and B. P. Stoicheff, Phys. Rev. **180**, 61 (1969).
[6]Ya. S. Bobovich and A. V. Bortkevich, Usp. Fiz. Nauk **103**, 3 (1971) [Sov. Phys. Usp. **14**, 1(1971–72)].
[7]Ya. S. Borovich, A. V. Bortkevich, and V. V. Kryukov, Opt. Spektrosk. **30**, 257 (1971) [Opt. Sepctrosc. **30**, 137 (1971)].
[8]E.I. Kazakova, A. V. Kraiskiĭ, V. A. Zubov, M. M. Sushchinskiĭ, and I. K. Shuvalov, Kr. Soobshch. Fiz. No. 7, 42 (1970).
[9]G. V. Peregudov, E. N. Ragozin, and V. A. Chirkov, Zh. Eksp. Teor. Fiz. **63**, 421 (1972) [Sov. Phys. JETP **36**, 223 (1973)].
[10]A. V. Kraiskiĭ, Kr. Soobshch. Fiz. No. 7, 42 (1970).
[11]M. M. Sushchinskiĭ, Stimulated Light Scttering (in Russian), Nauka, M., 185.

[12]S. A. Akhmanov, V. I. Emel'yanov, N. I. Koroteev, and V. N. Seminogov, Usp. Fiz. Nauk **147**, 675 (1985) [Sov. Phys. Usp. **28**, 1084 (1985)].
[13]A. Schuster, Astrophys. J. **21**, 1 (1905).
[14]A. A. Gershun, Tr. Gos. Opt. Inst. **11**, No. 99, 43 (1936).
[15]V. N. Denisov, B. N. Mavrin, V. B. Podobedov, Kh. E. Sterin, and B. G. Varshal, Opt. Spektrosk. **49**, 406 (1980) [Opt. Spectrosc. **49**, 221 (1980)].
[16]R. M. Martin and L. M. Falicov, in: *Light Scattering in Solids* (ed. M. Cardona), Springer-Verlag, New York, 1975, p. 80 [Russ transl., Mir, M., 1979, p. 101].
[17]M. M. Sushchinskiĭ, Raman Spectra of Molecules and Crystals, Israel Program for Scientific Translations, Jerusalem, 1973 [Russ. original, Nauka, M., 1969].
[18]D. L. Rousseau, J. M. Friedman, and P. F. Williams, in: *Raman Spectroscopy of Gases and Liquids* (ed. A. Weber), Springer-Verlag, New York, 1979, p. 203 [Russ. transl., Mir, M., 1982, p. 247].
[19]D. A. Long and L. Stanton, Proc. Roy. Soc. Ser. A **318**, 441 (1970).
[20]P. P. Shorygin, Dokl. Akad. Nauk SSSR **87**, 201 (1952).
[21]P. P. Shorygin, Usp. Fiz. Nauk **109**, 293 (1973) [Sov. Phys. Usp. **16**, 99 (1973–74)].
[22]V. S. Ryazanov and M. M. Sushchinskiĭ, Opt. Spektrosk. **23**, 580 (1967) [Opt. Spectrosc. **23**, 312 (1967)].
[23]V. S. Ryazanov and M. M. Sushchinskiĭ, Zh. Eksp. Teor. Fiz. **54**, 1099 (1968) [Sov. Phys. JETP **27**, 589 (1968)].
[24]A. S. Zhdanova, V. S. Gorelik, and M. M. Sushchinskiĭ, Opt. Spektrosk. **31**, 903 (1971) [Opt. Spectrosk. **31**, 490 (1971)].
[25]L. A. Shelepin, Zh. Eksp. Teor. Fiz. **54**, 1463 (1968) [Sov. Phys. JETP **27**, 784 (1968)].
[26]R. C. Miller, Phys. Rev. A **134**, 1313 (1964).
[27]V. S. Gorelik, O. P. Maksimov, G. G. Mitin, and M. M. Sushchinskiĭ, Fiz. Tverd. Tela (Leningrad) **15**, 1688 (1973) [Sov. Phys. Solid State **15**, 1133 (1973)].
[28]G. G. Mitin, V. S. Gorelik, B. N. Matsonashvili, and M. M. Sushchinskiĭ, Fiz. Tverd. Tela (Leningrad) **16**, 1262 (1974) [Sov. Phys. Solid State **16**, 817 (1974)].
[29]C. H. Perry and D. B. Hall, Phys. Rev. Lett. **15**, 14 (1965).
[30]W. I. Merz, Phys. Rev. **91**, 513 (1953).
[31]Ya. S. Bobovich and A. V. Bortkevich, Zh. Prikl. Spektrosk. **9**, 162 (1968) [J. Appl. Spectrosc. **9**, 750 (1968)].
[32]Ya. S. Bobovich and A. V. Bortkevich, Zh. Prikl. Spektrosk. **11**, 662 (1969) [J. Appl. Spectrosc. **11**, 1200 (1969)].
[33]A. B. Bortkevich and Ya. S. Bobovich, Zh. Prikl. Spektrosk. **10**, 992 (1969) [J. Appl. Spectrosc. **10**, 673 (1969)].
[34]A. I. Sokolovskaya, A. D. Kudryavtseva, T. P. Zhbanova, and M. M. Sushchinskiĭ, Zh. Eksp. Teor. Fiz. **53**, 429 (1967) [Sov. Phys. JETP **26**, 286 (1968)].
[35]A. I. Sokolovskaya, A. D. Kudryavtseva, G. L. Brekhovskikh, and M. M. Sushchinskiĭ, Zh. Eksp. Teor. Fiz. **57**, 1160 (1969) [Sov. Phys. JETP **30**, 633 (1970)].
[36]Ya. S. Bobovich and A. V. Bortkevich, Kvant. Elektron. **4**, 485 (1977) [Sov. J. Quantum Electron. 7, 269 (1977)].
[37]**NOT TRANSLATED**— The above is 36, not 37, as listed in English Manuscript because the numbers 4, 485, and date (1977) appear in the Russian in Ref. 36.
[38]T. Englert, G. Abstreiter, and I. Pontcharra, Sol. State Electron. **23**, 31 (1980).
[39]V. S Gorelik, R. N. Khashimov, A. P. Vidanov, and V. N. Mikhailov, Kr. Soobshch. Fiz. No. 6, 18 (1984) [Sov. Phys. Lebedev Inst. Rep. No. 6, 17 (1984)].
[40]E. A. Vinogradov, G. N. Zhizhin, T. A. Leskova, N. N. Mel'nik, and V. K. Yudson, Zh. Eksp. Teor. Fiz. **78**, 1030 (1980) [Sov. Phys. JETP **51**, 520 (1980)].
[41]V. S. Gorelik, M. M. Sushchinskiĭ, and R. N. Khashimov, Resonant Raman Scattering in Submicron Epitaxial Films and Implanted Silicon Layers, Preprint No. 15 Fiz. Inst. Akad. Nauk SSSR, M., 1985.
[42]M. M. Suschinskiĭ and V. S. Gorelik, J. Raman Spectr. **17**, 161 (1986).
[43]G. Contreras, A. K. Good, M. Cardona, and A. Compan, Sol. State Commun. **49**, 303 (1984).
[44]D. E. Aspnes and A. A.Studna, Phys.Rev. B **27**, 985 (1983).
[45]R. N. Khashimov, Raman Scattering in Deformed Submicron Films and Near-Surface Layers of Diamond Lattice Crystals, Author's Abstract, Doctoral Dissertation, Fiz. Inst. Akad. Nauk SSSR, M., 1986.
[46]E. Anastassakis, A. Pinczuk, E. Burstein, F. H. Pollak, and M. Cardona, Sol. State Commun. **8**, 133 (1970).
[47]V. G. Khamdamov, I. I. Novak, and V. I. Vettegren', Fiz. Tverd. Tela (Leningrad) **26**, 327 (1984) [Sov. Phys. Solid State **26**, 195 (1984)].
[48]N. Bloembergen, *Nonlinear Optics*, Benjamin, New York, 1965 [Russ. transl., Mir, M., 1966].
[49]M. Cardona, in: *Light Scattering in Solids*, Vol. II (ed. M. Cardona and G. Güntherodt), Springer-Verlag, New York, 1982, p. 19 [Russ. transl., Mir, Moscow, 1984, p. 35].
[50]H. Vogt, *Light Scattering in Solids*, Vol. II (ed. M. CArdona and G. Güntherodt), Springer-Verlag, New York, p. 208 [Russ. transl., Mir, Moscow, 1984, p. 277].
[51]C. Weisbuch and R. G. Ulbrich, *Light Scattering in Solids, Vol. III* (ed. M. Cardona and G. Güntherodt), Springer-Verlag, New York, 1982, p. 186 [Russ transl., Mir, Moscow, 1984, p. 228].
[52]G. R. Wilkinson, in: The Raman Effect, Vol. 2, Applications, ed. A. Anderson, Marcel Dekker, N.Y., 1973, p. 811 [Russ. transl., Mir, M., 1977, p. 408].
[53]P. P. Shorygina and L. N. Ovander, Current Problems in Raman Spectroscopy (in Russian), Nauka, M., 1973, p. 256.
[54]R. M. Martin and T. C. Damen, Phys. Rev. Lett. **26**, 86 (1971).
[55]R. C. C. Leite and S. P. S. Porton, Phys. Rev. Lett. **17**, 12 (1966).
[56]R. C. C. Leite, J. F. Scott, and T. C. Damen, Phys. Rev. Lett. **22**, 780 (1969).
[57]I. M. Ralston, R. L. Wadsack, and R. K. Chang, Phys. Rev. Lett. **25**, 814 (1970).
[58]V. S. Gorelik, O. G. Zolotukhin, and M. M. Sushchinskiĭ, Fiz. Tekhnol. Poluprovodn. **17**, 1157 (1983) [Sov. Phys. Semicond. **17**, 730 (1983)].
[59]P. I. Colwell and M. V. Klein, Sol. State Commun. **8**, 2095 (1970).
[60]M. M. Sushchinskiĭ, Kr. Soobshch, Fiz. No. 2, 3 (1972).
[61]Yu. N. Polivanov and R. Sh. Sayakhov, Pis'ma Zh. Eksp. Teor. Fiz. **30**, 617 (1979) [Sov. Phys. JETP **30**, 580 (1979)].
[62]Yu. N. Polivanov and R. Sh. Sayakhov, Kvant. Elektron. **6**, 2485 (1979) [Sov. J. Quantum Electron. **9**, 1472 (1979)].
[63]Yu. N. Polivanov and R. Sh. Sayakhov, Kr. Soobshch. Fiz. No. 8, 31 (1979) [Sov. Phys. Lebedev Inst. Rep. No. 8, 26 (1979)].
[64]A. M. Agal'tsov, V. S. Gorelik, and M. M. Sushchinskiĭ, Opt. Spektrosk. **58**, 386 (1985) [Opt. Spectrosc. **58**, 230 (1985)].
[65]A. F. Penne, A. Chaves, P. Andrade, and S. P. S. Porto, Phys. Rev. B **13**, 4907 (1976).
[66]V. S. Gorelik, O. G. Zolotukhin, and M. M. Sushchinskiĭ, Fiz. Tverd. Tela (Leningrad) **22**, 1024 (1980) [Sov. Phys. Solid State **20**, 598 (1980)].
[67]M. M. Sushchinskiĭ, Tr. Fiz. Inst. Akad. Nauk SSSR **132**, 3 (1982).
[68]M. M. Sushchinskiĭ, Raman scattering in crystals, Preprint No. 284 Fiz. Inst. Akad. Nauk SSSR, M., 1982.
[69]V. N. Denisov, B.N. Mavrin, V. B. Podobedov, and Kh. E. Sterin, Zh. Eksp. Teor. Fiz. **75**, 684 (1978) [Sov. Phys. JETP **48**, 344 (1978)].
[70]V. S. Gorelik, O. G. Zolotukhin, T. V. Moskaleva, and M. M. Sushchinskiĭ, Kvant. Elektron. **10**, 1949 (1983) [Sov. J. Quantum Electron. **13**, 1300 (1983)].
[71]B. N. Mavrin, Spectroscopy of Hyper-Raman Scattering by Vibrational Excitations in Crystals, Glasses, and Liquids, Author's Abstract, Doctoral Dissertation, Inst. Spektrosk. Akad. Nauk SSSR, Troitsk, 1984.
[72]V. N. Denisov, Hyper-Raman Scattering by Phonons in Alkali Halide Crystals, Preprint No. 4 Inst. Spektrosk. Akad. Nauk SSSR, M., 1984.
[73]I. F. Morhange, G. Kanellis, and M. Balkanski, Sol. State Commun. **31**, 805 (1979).
[74]V. M. Agranovich, Usp. Fiz. Nauk **115**, 199 (1975) [Sov. Phys. Usp. **18**, 99 (1975)].
[75]D. I. Evans, S. Uschoida, and I. D. McMullan, Phys. Rev. Lett. **31**, 369 (1973).
[76]V. S. Gorelik, V. B. Divak, and M. M. Sushchinskiĭ, Kr. Soobshch. Fiz. No. 4, 17 (1982) [Sov. Phys. Lebedev Inst. Rep. No. 4, 13 (1982)].

Translated by A. Zaslavsky